

Source apportionment of elemental carbon in Beijing, China: insights from radiocarbon and organic marker measurements

Yanlin Zhang, Jürgen Schnelle-Kreis, Guelcin Abbaszade, Ralf Zimmermann, Peter Zotter, Rong-rong Shen, Klaus Schaefer, Longyi Shao, Andre Prevot, and Soenke Szidat

Environ. Sci. Technol., **Just Accepted Manuscript** • DOI: 10.1021/acs.est.5b01944 • Publication Date (Web): 26 Jun 2015

Downloaded from <http://pubs.acs.org> on July 1, 2015

Just Accepted

“Just Accepted” manuscripts have been peer-reviewed and accepted for publication. They are posted online prior to technical editing, formatting for publication and author proofing. The American Chemical Society provides “Just Accepted” as a free service to the research community to expedite the dissemination of scientific material as soon as possible after acceptance. “Just Accepted” manuscripts appear in full in PDF format accompanied by an HTML abstract. “Just Accepted” manuscripts have been fully peer reviewed, but should not be considered the official version of record. They are accessible to all readers and citable by the Digital Object Identifier (DOI®). “Just Accepted” is an optional service offered to authors. Therefore, the “Just Accepted” Web site may not include all articles that will be published in the journal. After a manuscript is technically edited and formatted, it will be removed from the “Just Accepted” Web site and published as an ASAP article. Note that technical editing may introduce minor changes to the manuscript text and/or graphics which could affect content, and all legal disclaimers and ethical guidelines that apply to the journal pertain. ACS cannot be held responsible for errors or consequences arising from the use of information contained in these “Just Accepted” manuscripts.

1 **Source apportionment of elemental carbon in Beijing, China: insights from**
2 **radiocarbon and organic marker measurements**

3 Yan-Lin Zhang^{1,2,3*}, Jürgen Schnelle-Kreis⁴, Gülcin Abbaszade⁴, Ralf Zimmermann^{4,5},
4 Peter Zotter^{2, #}, Rong-rong Shen⁶, Klaus Schäfer⁶, Longyi Shao⁷, André S.H. Prévôt² and
5 Sönke Szidat¹

6 ¹Department of Chemistry and Biochemistry & Oeschger Centre for Climate Change
7 Research, University of Bern, 3012 Berne, Switzerland

8 ²Paul Scherrer Institute (PSI), 5232 Villigen-PSI, Switzerland

9 ³Yale-NUIST Center on Atmospheric Environment, Nanjing University of Information
10 Science and Technology, 210044, Nanjing, China

11 ⁴Joint Mass Spectrometry Center, Cooperation Group Comprehensive Molecular
12 Analytics, Helmholtz Zentrum München, 85764 Neuherberg, Germany

13 ⁵Joint Mass Spectrometry Centre, Chair of Analytical Chemistry, Institute of Chemistry
14 University of Rostock, 18059 Rostock, Germany

15 ⁶Institute of Meteorology and Climate Research (IMK-IFU), Karlsruhe Institute of
16 Technology (KIT), 82467 Garmisch-Partenkirchen, Germany

17 ⁷State Key Laboratory of Coal Resources and Safe Mining, School of Geoscience and
18 Surveying Engineering, China University of Mining and Technology (Beijing), Beijing
19 100083, China.

20 [#] now at: Lucerne School of Engineering and Architecture, Bioenergy Research, Lucerne
21 University of Applied Sciences and Arts, 6048 Horw, Switzerland

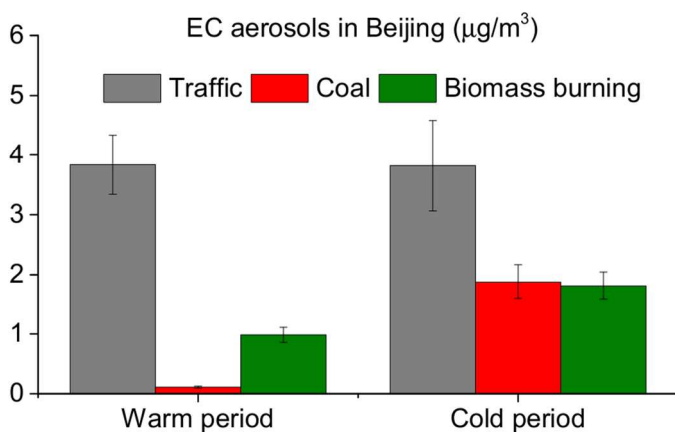
22 ^{*} To whom correspondence should be addressed. Email: dryanlinzhang@gmail.com

23 Phone: +41 31 631 4308 FAX: +41 31 631 43 99

24 Abstract

25 Elemental carbon (EC) or black carbon (BC) in the atmosphere has a strong influence on
26 both climate and human health. In this study, radiocarbon (^{14}C) based source
27 apportionment is used to distinguish between fossil fuel and biomass burning sources of
28 EC isolated from aerosol filter samples collected in Beijing from June 2010 to May 2011.
29 The ^{14}C results demonstrate that EC is consistently dominated by fossil-fuel combustion
30 throughout the whole year with a mean contribution of $79\% \pm 6\%$ (ranging from 70% to
31 91%), though EC has a higher mean and peak concentrations in the cold season. The
32 seasonal molecular pattern of hopanes (i.e. a class of organic markers mainly emitted
33 during the combustion of different fossil fuels) indicates that traffic-related emissions are
34 the most important fossil source in the warm period and coal combustion emissions are
35 significantly increased in the cold season. By combining ^{14}C based source apportionment
36 results and picene (i.e. an organic marker for coal emissions) concentrations, relative
37 contributions from coal and vehicle to EC in the cold period were estimated as $25\pm 4\%$
38 and $50\pm 7\%$, respectively, whereas the coal combustion contribution was negligible or
39 very small in the warm period.

40 TOC



41

42 1 Introduction

43 Atmospheric aerosols adversely affect human health by causing respiratory and
44 cardiopulmonary diseases associated with increased morbidity and mortality [1, 2].
45 Carbonaceous components are a major fraction of atmospheric aerosols and are often

46 classified into the sub-fractions organic carbon (OC) and elemental carbon (EC) or black
47 carbon (BC) [3]. In this study, BC is used as a qualitative and descriptive term not
48 referring to measurement results of any specific properties, whereas BC mass quantified
49 by thermal-optical methods is specified as EC [4]. As the major light-absorbing part of
50 carbonaceous material, BC exhibits the second largest anthropogenic radiative forcing
51 after carbon dioxide (CO₂) [5]. Recently, it was estimated that 640 - 4900 premature
52 human deaths could be prevented annually by utilizing available mitigation measures to
53 reduce BC in the atmosphere [6]. Due to a relatively short life time (~days) in atmosphere,
54 reducing BC emissions may rapidly improve both climate and human health [7, 8].
55 Therefore, the identification and quantification of different BC sources and their emission
56 source strengths is crucial for the implementation of effective mitigation strategies.

57 The emission sources of BC are exclusively combustion processes of fossil and non-fossil
58 fuels, although the relative contribution of these two sources still remains uncertain. In
59 recent years, the radiocarbon (¹⁴C) measurement of EC has been proven to be a powerful
60 tool for the differentiation between modern (i.e. biomass burning) and fossil (i.e. traffic
61 and coal) sources. ¹⁴C is completely depleted in fossil fuel emissions due to its half-life
62 (i.e. 5730 years), whereas ¹⁴C in non-fossil carbonaceous materials contains a similar
63 composition as atmospheric CO₂ [9, 10]. Therefore, ¹⁴C measurement of the EC fraction
64 directly enables the quantification of its biomass-burning and fossil sources [11].
65 However, the ¹⁴C measurement of EC still remains challenging in comparison to total
66 carbon (TC) due to its complex properties [12] and since a clear physical separation
67 between OC and EC is necessary to avoid artefacts in the ¹⁴C signal. Nevertheless, recent
68 developments and method adaptations from different groups show more consistent
69 approaches and yield more robust ¹⁴C results [13, 14].

70 Beijing, the capital of China with about 19.6 million inhabitants in 2010, is one of the
71 largest cities in the world and has become a heavily polluted area due to rapid
72 urbanization and industrialization over the past two decades [15]. In the last decade,
73 many studies have reported the chemical composition and sources of aerosols in Beijing
74 [16-23]. Most of these studies have focused on source apportionment of organic aerosols
75 (organic matter, OM or OC) by positive matrix factorization (PMF) [24] and chemical

76 mass balance (CMB) models [21] from off-line organic markers measurement or online
77 aerosol mass spectrometer measurement. However, only a few studies have reported
78 year-round source apportionment results of BC. For example, Duan et al. (2004)
79 demonstrated biomass burning and traffic and/or industry emissions are the major sources
80 of both OC and EC during summer, while coal combustion is the dominant contributor
81 during the winter heating period, although quantification of contributions from each
82 source still remains uncertain. Based on PMF model analysis, about 50% of OC and EC
83 in Beijing were associated with biomass-burning processes [25]. In contrast, most recent
84 source-diagnostic ^{14}C studies suggested ~80% contribution from fossil fuels in winter for
85 EC in China [15, 23, 26]. A quantitative understanding of the temporal variations and
86 source apportionment of EC in Beijing is still missing and thus crucially necessary. In
87 this study, we determine fossil and biomass-burning contributions to year-round EC
88 aerosols in Beijing by measuring ^{14}C of EC and organic markers for fossil emissions (i.e.
89 hopanes and picene).

90 **2 Experimental**

91 **2.1 Sampling**

92 24-h integrated PM₄ samples (n=155) were collected at the ground level on pre-baked
93 (650 °C, 4 h) quartz-fibre filters (diameter: 150mm) using a high-volume sampler (Digitel
94 DHA-80, Switzerland) at a flow rate of ~167 l/min during June 2010 to May 2011 at the
95 campus of the China University of Geosciences, a residential area in North West of
96 Beijing. It should be noted that during the whole campaign the actual sampling flow of
97 ambient air was 167 instead of 500 l/min as a default setting due to an airflow shortcut
98 from the interior of the sampler. As a consequence to the changed flow volume, the cut
99 off of the sampler (original setting: 2.5 μm) had to be recalculated following the impactor
100 design theory [27, 28]. It was found that particles smaller than 4 μm (i.e., PM₄) were
101 collected onto the filters. However, a comparison of ^{14}C results obtained from the current
102 study was not significantly different from those found for PM_{2.5} samples during winter
103 2013 (see Supplementary information, Figure S1) [29]. Our previous work has also
104 shown that there is no significant difference of EC source signatures (fossil vs. non-fossil)

105 between PM₁, PM_{2.5} and PM₁₀ at other locations (Table S1) [30]. Further, since EC
106 almost exclusively derives from combustion sources, the size of EC particles from
107 China's source samples is mostly smaller than 1 μm [31, 32] and the majority of EC mass
108 (~80%) in urban site of China resides in particles smaller than 3.2 μm in diameter and
109 the fine mode peaks at around either 0.42 μm or 0.75 μm [33]. As a result, the cut size
110 present in our study generally would not affect the results of relative fossil and non-fossil
111 contribution of EC of aerosols because EC is dominated in the fine particles. After
112 sampling, filters were wrapped in aluminum foil and stored in a freezer at -20°C before
113 analysis. Every second week, one field blank was collected.

114 **2.2 Elemental carbon measurement**

115 A filter cut of 1.5 cm^2 was used for EC measurement. The EC concentrations were
116 measured using a thermo-optical OC/EC analyzer (Model 4L, Sunset Laboratory Inc,
117 USA), equipped with a non-dispersive infrared (NDIR) detector following the thermal-
118 optical transmittance protocol (TOT) EUSAAR2 [34]. A high uncertainty of 20% is
119 considered for all measured EC concentrations to account for possible differences
120 between different TOT protocols [35, 36]. It should be noted that only the absolute EC
121 concentration is affected by this additional uncertainty, whereas the relative fossil and
122 non-fossil contribution is only influenced by the combined uncertainty of the
123 ^{14}C measurement of EC and the bomb peak correction, which is on average 5% (see
124 below). No EC was detected on blank filters and consequently no blank correction was
125 necessary.

126 **2.3 Radiocarbon (^{14}C) measurement of EC**

127 A filter cut of 1 to 6 cm^2 (corresponding to 5 to 30 μgC) was used for ^{14}C analysis. The
128 Swiss_4S protocol was applied for the EC isolation for the ^{14}C analysis using a Sunset
129 OC/EC analyzer connected to a gas preparation line as described by [14]. This special
130 protocol is optimized to minimize the bias in the ^{14}C result of EC from OC charring or
131 losses of the least refractory EC during the OC removal. In brief, to minimize positive
132 artefacts from OC charring, water-soluble OC is first eliminated by a water-extraction
133 pre-treatment and the remaining water-insoluble OC is then removed using the Sunset

134 OC/EC analyzer with a thermal treatment in three steps: (1) 375 °C for 150 s in pure
135 oxygen (O₂); (2) 475 °C for 180 s in O₂; (3) 450 °C for 180 s followed by 180 s at 650 °C
136 in helium. Finally, in step four EC is isolated by the combustion of the remaining
137 carbonaceous material at 760 °C for 150 s in O₂. EC recovery is estimated by the ratio
138 ATN_t/ATN_0 , where ATN_0 is the initial attenuation (ATN, see Supporting Information),
139 which is related to the total amount of EC on the filter, and ATN_t is the attenuation at the
140 time t , when the EC step (i.e., step 4) begins. By using the Swiss_4S protocol, OC
141 charring is minimized to 4±3% compared to EC (see Supporting Information), which
142 may lead a negligible overestimation of non-fossil EC by less than 3%. This assures the
143 accuracy of ¹⁴C measurement in EC. The EC recovery in this study was estimated as
144 85±5%, thus presenting almost the entire continuum of EC. ¹⁴C results in EC were
145 extrapolated to 100% EC recovery ($f_{M,EC,corrected} = slope * (1 - EC\ recovery) + f_{M,EC}$) to
146 account for the less refractory EC, mainly from wood burning, which is removed during
147 steps 1 to 3 [14]. The slope of 0.31 is deduced from linear regression of the EC recovery
148 and $f_{M,EC}$ [14]. The uncertainty of the reported $f_{M,EC}$ is obtained by an error propagation
149 of all possible uncertainties including an assigned uncertainty of 10% for the slope, the
150 measurement uncertainty of $f_{M,EC}$ (2%) and an assigned uncertainty of 10% for the EC
151 yield, which results to a total average uncertainty of 4 %.

152 The evolving CO₂ in step 4 was separated from interfering gaseous products, cryo-
153 trapped and sealed in glass ampoules for ¹⁴C measurements. ¹⁴C measurements of the
154 CO₂ was carried out with the **M**ini radio**C**arbon **D**ating System, MICADAS [37] using
155 a gas ion source [38]. The ¹⁴C results are presented as fraction of modern (f_M) denoting
156 the ¹⁴C/¹²C content of the sample related to that of the reference year 1950 [39]. Oxalic
157 acid (HOxII) reference material ($f_M=1.3407$) and of ¹⁴C-free materials ($f_M=0$) are used for
158 normalization background correction. The f_M values were further corrected for $\delta^{13}C$
159 fractionation and for ¹⁴C decay between 1950 and the year of measurement [40]. The f_M
160 measurement uncertainty for the EC samples is ~2%.

161 2.4 Organic marker (hopanes and picene) measurements

162 A filter cut of 1-6 cm² was used for organic marker's measurement. The organic markers
163 picene and hopanes (see Table 2) were quantified using in-situ derivatization thermal
164 desorption gas-chromatography time of flight mass spectrometry (IDTD-GC-MS,
165 Orasche et al. [41]). Briefly, the filter punches were placed into glass liners suitable for
166 an automated thermal desorption unit. Isotope-labelled standard compounds were spiked
167 directly onto the filter surface to account for influences of the matrix for later
168 quantification. Derivatization was performed on the filter by adding of liquid
169 derivatization reagent N-methyl-N-trimethylsilyl-tri fluoroacetamide (MSTFA,
170 Macherey-Nagel, Germany). During 16 min of desorption time, in addition an in-situ
171 derivatization with gaseous MSTFA was carried out. Desorbed molecules were trapped
172 on a pre-column before separation by gas chromatography (BPX-5 capillary column,
173 SGE, Australia). The detection and quantification of compounds was carried out on a
174 Pegasus III time-of-flight mass spectrometer (TOF) using the ChromaTOF software
175 package (LECO, St. Joseph, MI). The blank values of hopanes and picene were below the
176 detection limit (0.02 ng/m³).

177

178 3 Results and Discussions

179 3.1 Temporal variation of EC

180 Figure 1 shows EC concentrations during the whole sampling period. EC concentrations
181 range from 0.8 to 11.8 µg/m³, and the average of 4.0±2.2 µg/m³ is within the range
182 (2.3~7.4 µg/m³) reported by previous studies for Beijing [21, 42]. The EC concentrations
183 are significantly lower (t-test with $p<0.05$) during the warm period (i.e. average from
184 March to October is 3.6±1.5 µg/m³) than in the cold period (i.e. average from November
185 to February is 4.8±2.9 µg/m³). It should be noted that the frequency of samples with EC
186 larger than 4.5 µg/m³ in the cold period is much larger than that in the warm period,
187 indicating a higher primary particulate pollution from enhanced anthropogenic emissions
188 during the cold period. A similar seasonal trend was also observed by [43]. This

189 seasonality is likely attributed to increased emissions from residential heating using coal
190 or biofuel. The lower EC abundance in the warm period is mainly caused by reduced
191 heating-related coal/biofuel emissions on the one hand and a higher mixing layer on the
192 other hand. It should be pointed out that EC concentration in summer at the studied site is
193 still higher than those observed in many other cities during summer such as Barcelona,
194 Spain ($1.2 \mu\text{g}/\text{m}^3$) [44], Paris, France ($1.4 \mu\text{g}/\text{m}^3$) [45] or Pittsburgh, USA ($0.89 \mu\text{g}/\text{m}^3$)
195 [46].

196 3.2 ^{14}C results of EC: fraction of modern

197 In order to further investigate the sources of EC, fourteen samples from different seasons
198 were selected for the analysis of ^{14}C of the EC fraction (Table 1). In order to address the
199 air quality problems of Beijing [15], we characterized EC sources for days with medium
200 and heavy air pollution during the warm and cold periods. Therefore, samples were
201 selected for radiocarbon analysis with EC concentrations $>3 \mu\text{g}/\text{m}^3$, which includes about
202 2/3 of all daily samples shown in Figure. 1, representing $\sim 82\%$ of the integrated EC
203 burden of all samples. However, EC sources of background days are not considered. The
204 values for $f_{\text{M}}(\text{EC})$ ranged from 0.10 to 0.34 with a mean of 0.23 ± 0.06 , indicating a
205 dominance of fossil sources of EC in Beijing throughout the year. Since EC is only
206 emitted as primary aerosol by combustion from either biomass or fossil fuels (i.e. coal
207 and vehicle emissions), $f_{\text{M}}(\text{EC})$ particularly tracks the change of EC sources. The lowest
208 $f_{\text{M}}(\text{EC})$ is found in summer (0.15), indicating the importance of vehicle emissions since
209 the coal consumption is much reduced compared to other seasons. $f_{\text{M}}(\text{EC})$ is higher by 60%
210 in the rest of the year than in summer, suggesting that EC from biomass burning becomes
211 substantial during the other seasons. Further discussions of source apportionment of fossil
212 EC will be presented in Sec. 3.4.

213 3.3 Fossil vs. biomass burning EC

214 The fraction of modern (f_{M}) is not identical to the fraction of non-fossil (f_{NF}) due to
215 increased ^{14}C content of the atmosphere from the nuclear bomb test in the 1950s and
216 1960s. A reference value representing the modern ^{14}C content of biomass burning

217 aerosols ($f_{M,bb}$) during the sampling period compared to 1950 before the bomb test is
218 used to convert f_M to f_{NF} :

$$219 \quad f_{NF}(EC) = f_M(EC) / f_{M,bb} \quad (\text{Eq. 1})$$

220 The value of $f_{M,bb}$ is estimated as 1.12 ± 0.05 [47]. Since biomass burning (including
221 biofuel combustion) is the only source of non-fossil EC, the fraction of non-fossil (f_{NF})
222 equals to the fraction of biomass burning (f_{BB}). The fraction of fossil fuels (f_{FF}) is
223 determined by:

$$224 \quad f_{FF} = 1 - f_{BB} \quad (\text{Eq. 2})$$

225 Fossil-fuel and biomass-burning EC concentrations (i.e. EC_{FF} and EC_{BB} , respectively) are
226 calculated as follows:

$$227 \quad EC_{FF} = EC * (1 - f_{BB}) \quad (\text{Eq. 3})$$

$$228 \quad EC_{BB} = EC * f_{BB} \quad (\text{Eq. 4})$$

229 Figure 2 shows the source apportionment results of EC. The EC_{FF} concentrations range
230 from 2.5 to 7.5 $\mu\text{g}/\text{m}^3$, whereas the corresponding range for EC from biomass burning
231 (EC_{BB}) was 0.4 to 2.4 $\mu\text{g}/\text{m}^3$. EC_{FF} values are on average 4.6 times higher than EC_{BB} ,
232 corresponding to a mean contribution of EC_{FF} to total EC of $79\% \pm 6\%$ (ranging from 70%
233 to 91%). The measured fossil contributions to EC are comparable to those previously
234 reported with a similar ^{14}C -based approach in Beijing during winter 2011 [48] and winter
235 2013 [29], but are higher than for an urban site in Guangzhou, China (winter 2012/2013:
236 $71 \pm 10\%$) [49] and a background site on the Hainan Island, South China (annual average
237 2005/2006: 25-56%) [47] as well as 16 urban and rural sites across Switzerland (winter
238 2007/2008–2011/2012: 13-88%) [11]. Higher EC_{FF} concentrations were observed in the
239 cold period, most probably associated with larger coal combustion for heating. However,
240 relative contributions from fossil combustion are even lower in the cold season than in
241 the warm season, implying that biomass-burning emissions are also considerably
242 important for the EC increment in the cold season. It should be noted that it is common
243 practice to burn maize and wheat residues especially in the rural areas without central
244 space heating and gas supplying systems and a large fraction of this biomass burning is

245 emitted as OC and EC [50]. The contribution of these biomass-burning emissions to EC
246 in cold seasons is likely very important due to lower combustion efficiency for residential
247 biomass burning than for coal boilers. By subtracting mean values of EC_{BB} and EC_{FF} in
248 the warm period from those in the cold period, the excess is estimated as 0.82 ± 0.40
249 $\mu\text{g}/\text{m}^3$ and $1.75 \pm 0.52 \mu\text{g}/\text{m}^3$ for EC_{BB} and EC_{FF} , respectively. Biomass burning accounted
250 for on the average 32% of the excess during the cold period, which is significantly higher
251 than the contribution of EC_{BB} (19%) during the warm period, but lower than estimations
252 from PMF model analysis (50%) [25].

253 3.4 Fossil EC from coal combustion and vehicle emissions

254 Hopanes are abundant in crude oils, coal and lubricants [51]. They have been identified in
255 emissions from heating oil burning [52], coal burning [53] and vehicles [54]. Table 2
256 presents hopane concentrations in the warm and cold periods and the difference between
257 these two seasons. As shown in Figure 3 and Table 2, the total identified hopanes mass
258 concentrations show a clearly seasonal trend with maximum in the cold period
259 ($68.6 \pm 28.7 \text{ ng}/\text{m}^3$) and minimum in the warm period ($17.9 \pm 6.5 \text{ ng}/\text{m}^3$). The hopane
260 molecular patterns differ substantially with the type of the fossil source, and therefore
261 potentially allow a distinction of coal combustion and vehicle emissions [55, 56]. For
262 example, the ab-hopane/(ab-hopane+ba-hopanes) ratio (i.e. $30ab/(30ab+30ba)$) increases
263 with increasing diagenesis and catagenesis of the sediments. This ratio, also called
264 hopane index, is >0.9 in crude oil [57] and 0.1-0.6 in different types of coal [53, 58]. In
265 typical petroleum, the R/S-epimerization at C22 has an equilibrium S/(S+R) ratio, the so-
266 called homo-hopane index (i.e. $31abs/31abs+31abR$) of ~ 0.6 [59], whereas this ratio
267 ranges from about 0.1 for lignite coal to ~ 0.4 for bituminous coal. As seen in Table 2,
268 both the hopane index (0.84 ± 0.11) and the homo-hopane index (0.56 ± 0.04) in the warm
269 period are very close to those in vehicle exhausts, suggesting that contribution of coal
270 burning was negligible or very small in summer in Beijing. In contrast, both ratios found
271 in the cold period (0.57 ± 0.06 and 0.46 ± 0.07 for hopane index and the homo-hopane
272 index, respectively) are between those of petroleum and coal-burning emissions,
273 indicating additional fossil-fuel emissions from solid coal combustion. Moreover, picene
274 (a specific marker of coal combustion) was also determined in our study (Figure 3 and

275 Table 2) and considerable concentrations are observed during the cold period (i.e. ranging
276 from 0.34-4.48 ng/m³ with a mean of 1.82±0.99 ng/m³), in contrast to the warm period,
277 when concentrations were often below the detection limit or very small. If we assume
278 that meteorological factors (i.e. wind speed and boundary layer height) equally affected
279 both the EC_{FF} and picene concentrations then the difference between the cold and the
280 warm periods for EC_{FF} and picene (i.e. ΔEC_{FF} and Δpicene , respectively) can be
281 attributed only to additional coal combustion. This assumption is also supported by a
282 recent study, in which primary organic aerosols from traffic-related emissions were only
283 found to be ~10%, which was even smaller for high pollution events than for low
284 pollution events in winter Beijing [15]. The emission ratio picene/EC for coal combustion
285 is therefore estimated as 1.1 (ng/ μ g) by:

$$286 \quad (\text{picene/EC})_{\text{coal}} = \Delta \text{picene} / \Delta EC_{FF} \quad (\text{Eq. 5})$$

287 The uncertainty of $(\text{picene/EC})_{\text{coal}}$ is estimated to be 0.22 by an error propagation of
288 possible uncertainties including by assigning 10% as the uncertainty of Δpicene and 20%
289 as the uncertainty of ΔEC_{FF} associated with a overestimation of the EC_{coal} or EC_{traffic} in
290 winter.

291 It should be pointed out that picene may not be stable in summer [60], however, the
292 emission ratio estimated by our approach would only change by <3% if assuming 0-50%
293 of picene in summer has decayed through photochemical transformations. This emission
294 ratio is comparable to the calculated emission ratios for Chinese residential bituminous
295 coal (0.8) combustion but much lower than those found in residential anthracite (2.7), and
296 coal briquette (3.2) combustion [61]. Similarly, the hopane and homo-hopane indexes for
297 the excess between the cold and warm period is estimated as 0.49 and 0.35 (Table 2),
298 respectively, which are very close to those in residential combustion of bituminous coal
299 (0.52 and 0.37 for the hopane and homo-hopane indexes, respectively), but very different
300 from typical emission ratios in mineral-oil-based sources (i.e. fuel oil consumption and
301 vehicular emissions) (i.e. hopane index >0.9 and homohopane index in the range of 0.54-
302 0.67) [53, 56, 59]. This suggests that the bituminite is a dominant contributor of the
303 excess EC, which is associated with the highest EC emission factor from bituminous
304 coals compared to other coal types on one hand and a larger percentage (78%) of
305 bituminous coal in total raw coal in 2000 in China on the other hand [62].

306 The fraction of traffic and coal combustion to EC particles is further calculated by:

307 $EC_{\text{coal}} = \text{picene} / (\text{picene}/EC)_{\text{coal}}$ (Eq. 6)

308 $EC_{\text{traffic}} = EC_{\text{FF}} - EC_{\text{coal}}$ (Eq. 7)

309 The “best estimate” and its associated uncertainty are obtained by Latin-hypercube
310 sampling (LHS) [23]. This approach is comparable to Monte Carlo simulation which has
311 been reported in many ^{14}C -based source apportionment studies [63-66]. The emission
312 ratio of picene/EC for coal combustion or $(\text{picene}/EC)_{\text{coal}}$ may be overestimated by 25%
313 or underestimated by 50%, if the traffic EC in winter is actually lower or higher than that
314 in summer, respectively. Considering the overall uncertainty of $(\text{picene}/EC)_{\text{coal}}$, a range
315 from 0.75 to 1.5 with a central value of 1.0 is used as the input. The LHS simulation is
316 conducted by generating 3000 random sets of variables. Simulations producing negative
317 solutions are excluded and the median value from the remaining simulations is used as
318 the best estimate, and the 10th and 90th percentiles of the solutions are used as
319 uncertainties [23].

320 As shown in Figure 4, EC is divided into three major sources: EC_{BB} , EC_{traffic} and EC_{coal} .
321 The changes in the source pattern between the warm and cold season are substantial,
322 though vehicle emissions are the most important source of EC in both the warm and cold
323 periods with a mean contribution of $79 \pm 6\%$ and $50 \pm 7\%$, respectively. However, the
324 biomass-burning contribution slightly increased (from 19% to 24%) and the coal
325 combustion contribution increased dramatically in the cold period. The excess of EC
326 between the cold and warm seasons was shared by coal ($68 \pm 4\%$) and biomass burning
327 combustion ($32 \pm 4\%$) sources. The importance of coal contribution in the cold period is
328 also evident by the occurrence of picene and hopanes indices. The current results imply
329 that wintertime aerosol pollution in Beijing is likely driven by increased coal combustion
330 and possible secondary formation of other aerosol components such as nitrate, sulfate and
331 organic carbon co-emitted with EC [15, 29, 61, 67].

332 In summary, the sources of elemental carbon (EC) from ambient samples collected in
333 Beijing were investigated based on both radiocarbon (^{14}C) and organic marker
334 measurements. The results demonstrate that EC is dominated by fossil emissions

335 throughout the year with a mean contribution of $79\% \pm 6\%$. To further identify and
336 quantify traffic-related emissions and coal combustion contributions to fossil EC,
337 hopanes and picene were also measured. The concentrations of the total identified
338 hopanes are $68.6 \pm 28.7 \text{ ng/m}^3$ and $17.9 \pm 6.5 \text{ ng/m}^3$ in the cold and the warm period,
339 respectively. The seasonal molecular pattern of hopanes indicates that vehicle emissions
340 are the most important fossil source in the warm period and coal combustion emission is
341 increased significantly in the cold season. By combining the ^{14}C and organic marker's
342 measurements, relative contributions from coal and biomass-burning to the excess of EC
343 between the cold and warm seasons were estimated as 68% and 32%, respectively. Based
344 on published data from source samples, the hopane and home-hopane indexes as well as
345 the picene-to-EC ratios are compared among different kinds of coal types. The
346 comparison shows that the bituminite is a dominant coal type used during winter in
347 Beijing.

348 **Supporting Information**

349 Relevance of the charring reduction using the Swiss_4S protocol; table showing the
350 fraction of modern (f_M) of EC in PM1, PM2.5 and PM10 in Switzerland; figures
351 describing the fraction of modern (f_M) of EC in PM4 (winter, 2011) and PM2.5 (winter
352 2013) in Beijing, thermograms of water-extracted aerosol samples using Swiss_4S,
353 integrated probability distributions of the averaged relative contributions to EC from
354 different sources using the Latin-hypercube sampling (LHS) simulation, and the relative
355 contribution to EC from coal combustion (EC_{coal}) as a function of the selected
356 $(\text{picene}/\text{EC})_{\text{coal}}$. This material is available free of charge via the Internet
357 at <http://pubs.acs.org>.

358 The authors declare no competing financial interest.

359 **Acknowledgements**

360 Y.-L. Zhang acknowledges partial support from the Swiss National Science Foundation
361 Fellowship. This work is also partially supported by the KIT Centre for Climate and
362 Environment and the Helmholtz Zentrum München, German Research Center for

363 Environmental Health. R.-r. Shen acknowledges the PhD Scholarship from the China
364 Scholarship Council (CSC).

365 References

- 366 1. Pope III, C. A.; Dockery, D. W., Health effects of fine particulate air pollution:
367 Lines that connect. *J. Air Waste Manage. Assoc.* **2006**, *56*, (6), 709-742.
- 368 2. WHO, *Air Quality Guidelines: Global Update 2005: Particulate Matter, Ozone,*
369 *Nitrogen Dioxide and Sulfur Dioxide.* World Health Organization: 2006.
- 370 3. Jacobson, M. C.; Hansson, H. C.; Noone, K. J.; Charlson, R. J., Organic
371 atmospheric aerosols: Review and state of the science. *Rev. Geophys.* **2000**, *38*, (2), 267-
372 294.
- 373 4. Petzold, A.; Ogren, J. A.; Fiebig, M.; Laj, P.; Li, S. M.; Baltensperger, U.; Holzer-
374 Popp, T.; Kinne, S.; Pappalardo, G.; Sugimoto, N.; Wehrli, C.; Wiedensohler, A.; Zhang,
375 X. Y., Recommendations for reporting "black carbon" measurements. *Atmos. Chem. Phys.*
376 **2013**, *13*, (16), 8365-8379.
- 377 5. Ramanathan, V.; Carmichael, G., Global and regional climate changes due to
378 black carbon. *Nat. Geosci.* **2008**, *1*, (4), 221-227.
- 379 6. Weinhold, B., Global Bang for the Buck Cutting Black Carbon and Methane
380 Benefits Both Health and Climate. *Environ. Health Perspect.* **2012**, *120*, (6), A245-A245.
- 381 7. Shindell, D.; Kuylensstierna, J. C. I.; Vignati, E.; van Dingenen, R.; Amann, M.;
382 Klimont, Z.; Anenberg, S. C.; Muller, N.; Janssens-Maenhout, G.; Raes, F.; Schwartz, J.;
383 Faluvegi, G.; Pozzoli, L.; Kupiainen, K.; Hoglund-Isaksson, L.; Emberson, L.; Streets, D.;
384 Ramanathan, V.; Hicks, K.; Oanh, N. T. K.; Milly, G.; Williams, M.; Demkine, V.;
385 Fowler, D., Simultaneously Mitigating Near-Term Climate Change and Improving
386 Human Health and Food Security. *Science* **2012**, *335*, (6065), 183-189.
- 387 8. Bond, T. C.; Doherty, S. J.; Fahey, D. W.; Forster, P. M.; Berntsen, T.; DeAngelo,
388 B. J.; Flanner, M. G.; Ghan, S.; Karcher, B.; Koch, D.; Kinne, S.; Kondo, Y.; Quinn, P.
389 K.; Sarofim, M. C.; Schultz, M. G.; Schulz, M.; Venkataraman, C.; Zhang, H.; Zhang, S.;
390 Bellouin, N.; Guttikunda, S. K.; Hopke, P. K.; Jacobson, M. Z.; Kaiser, J. W.; Klimont,
391 Z.; Lohmann, U.; Schwarz, J. P.; Shindell, D.; Storelvmo, T.; Warren, S. G.; Zender, C.

- 392 S., Bounding the role of black carbon in the climate system: A scientific assessment. *J.*
393 *Geophys. Res.* **2013**, *118*, (11), 5380-5552.
- 394 9. Currie, L. A., Evolution and multidisciplinary frontiers of ^{14}C aerosol science.
395 *Radiocarbon* **2000**, *42*, (1), 115-126.
- 396 10. Szidat, S., Sources of Asian haze. *Science* **2009**, *323*, (5913), 470-471.
- 397 11. Zotter, P.; Ciobanu, V. G.; Zhang, Y. L.; El-Haddad, I.; Macchia, M.;
398 Daellenbach, K. R.; Salazar, G. A.; Huang, R. J.; Wacker, L.; Hueglin, C.; Piazzalunga,
399 A.; Fermo, P.; Schwikowski, M.; Baltensperger, U.; Szidat, S.; Prévôt, A. S. H.,
400 Radiocarbon analysis of elemental and organic carbon in Switzerland during winter-smog
401 episodes from 2008 to 2012 – Part 1: Source apportionment and spatial variability. *Atmos.*
402 *Chem. Phys.* **2014**, *14*, (24), 13551-13570.
- 403 12. Szidat, S.; Bench, G.; Bernardoni, V.; Calzolari, G.; Czimczik, C. I.; Derendorp, L.;
404 Dusek, U.; Elder, K.; Fedi, M.; Genberg, J.; Gustafsson, O.; Kirillova, E.; Kondo, M.;
405 McNichol, A. P.; Perron, N.; Santos, G. M.; Stenstrom, K.; Swietlicki, E.; Uchida, M.;
406 Vecchi, R.; Wacker, L.; Zhang, Y. L.; Prevot, A. S. H., Intercomparison of ^{14}C Analysis
407 of Carbonaceous Aerosols: Exercise 2009. *Radiocarbon* **2013**, *55*, (3–4), 1496-1509.
- 408 13. Bernardoni, V.; Calzolari, G.; Chiari, M.; Fedi, M.; Lucarelli, F.; Nava, S.;
409 Piazzalunga, A.; Riccobono, F.; Taccetti, F.; Valli, G.; Vecchi, R., Radiocarbon analysis
410 on organic and elemental carbon in aerosol samples and source apportionment at an
411 urban site in Northern Italy. *J. Aerosol Sci.* **2013**, *56*, 88-99.
- 412 14. Zhang, Y. L.; Perron, N.; Ciobanu, V. G.; Zotter, P.; Minguillón, M. C.; Wacker,
413 L.; Prévôt, A. S. H.; Baltensperger, U.; Szidat, S., On the isolation of OC and EC and the
414 optimal strategy of radiocarbon-based source apportionment of carbonaceous aerosols.
415 *Atmos. Chem. Phys.* **2012**, *12*, 10841-10856.
- 416 15. Huang, R. J.; Zhang, Y.; Bozzetti, C.; Ho, K. F.; Cao, J. J.; Han, Y.; Daellenbach,
417 K. R.; Slowik, J. G.; Platt, S. M.; Canonaco, F.; Zotter, P.; Wolf, R.; Pieber, S. M.; Bruns,
418 E. A.; Crippa, M.; Ciarelli, G.; Piazzalunga, A.; Schwikowski, M.; Abbaszade, G.;
419 Schnelle-Kreis, J.; Zimmermann, R.; An, Z.; Szidat, S.; Baltensperger, U.; El Haddad, I.;
420 Prevot, A. S., High secondary aerosol contribution to particulate pollution during haze
421 events in China. *Nature* **2014**, *514*, (7521), 218-22.

- 422 16. Sun, Y. L.; Zhuang, G. S.; Ying, W.; Han, L. H.; Guo, J. H.; Mo, D.; Zhang, W. J.;
423 Wang, Z. F.; Hao, Z. P., The air-borne particulate pollution in Beijing - concentration,
424 composition, distribution and sources. *Atmos. Environ.* **2004**, *38*, (35), 5991-6004.
- 425 17. Duan, F. K.; He, K. B.; Ma, Y. L.; Yang, F. M.; Yu, X. C.; Cadle, S. H.; Chan, T.;
426 Mulawa, P. A., Concentration and chemical characteristics of PM_{2.5} in Beijing, China:
427 2001-2002. *Sci. Tot. Environ.* **2006**, *355*, (1-3), 264-275.
- 428 18. Okuda, T.; Katsuno, M.; Naoi, D.; Nakao, S.; Tanaka, S.; He, K. B.; Ma, Y. L.;
429 Lei, Y.; Jia, Y. T., Trends in hazardous trace metal concentrations in aerosols collected in
430 Beijing, China from 2001 to 2006. *Chemosphere* **2008**, *72*, (6), 917-924.
- 431 19. Yang, F.; He, K.; Ye, B.; Chen, X.; Cha, L.; Cadle, S. H.; Chan, T.; Mulawa, P.
432 A., One-year record of organic and elemental carbon in fine particles in downtown
433 Beijing and Shanghai. *Atmos. Chem. Phys.* **2005**, *5*, 1449-1457.
- 434 20. Zhang, J. K.; Sun, Y.; Liu, Z. R.; Ji, D. S.; Hu, B.; Liu, Q.; Wang, Y. S.,
435 Characterization of submicron aerosols during a month of serious pollution in Beijing,
436 2013. *Atmos. Chem. Phys.* **2014**, *14*, (6), 2887-2903.
- 437 21. Zheng, M.; Salmon, L. G.; Schauer, J. J.; Zeng, L. M.; Kiang, C. S.; Zhang, Y. H.;
438 Cass, G. R., Seasonal trends in PM_{2.5} source contributions in Beijing, China. *Atmos.*
439 *Environ.* **2005**, *39*, (22), 3967-3976.
- 440 22. Sun, Y. L.; Jiang, Q.; Wang, Z. F.; Fu, P. Q.; Li, J.; Yang, T.; Yin, Y.,
441 Investigation of the sources and evolution processes of severe haze pollution in Beijing in
442 January 2013. *J. Geophys. Res.* **2014**, *119*, (7), 4380-4398.
- 443 23. Zhang, Y. L.; Huang, R. J.; El Haddad, I.; Ho, K. F.; Cao, J. J.; Han, Y.; Zotter, P.;
444 Bozzetti, C.; Daellenbach, K. R.; Canonaco, F.; Slowik, J. G.; Salazar, G.; Schwikowski,
445 M.; Schnelle-Kreis, J.; Abbaszade, G.; Zimmermann, R.; Baltensperger, U.; Prévôt, A. S.
446 H.; Szidat, S., Fossil vs. non-fossil sources of fine carbonaceous aerosols in four Chinese
447 cities during the extreme winter haze episode of 2013. *Atmos. Chem. Phys.* **2015**, *15*, (3),
448 1299-1312.
- 449 24. Sun, Y. L.; Zhang, Q.; Schwab, J. J.; Yang, T.; Ng, N. L.; Demerjian, K. L.,
450 Factor analysis of combined organic and inorganic aerosol mass spectra from high
451 resolution aerosol mass spectrometer measurements. *Atmos. Chem. Phys.* **2012**, *12*, (18),
452 8537-8551.

- 453 25. Cheng, Y.; Engling, G.; He, K. B.; Duan, F. K.; Ma, Y. L.; Du, Z. Y.; Liu, J. M.;
454 Zheng, M.; Weber, R. J., Biomass burning contribution to Beijing aerosol. *Atmos. Chem.*
455 *Phys.* **2013**, *13*, (15), 7765-7781.
- 456 26. Chen, B.; Du, K.; Wang, Y.; Chen, J. S.; Zhao, J. P.; Wang, K.; Zhang, F. W.; Xu,
457 L. L., Emission and Transport of Carbonaceous Aerosols in Urbanized Coastal Areas in
458 China. *Aerosol and Air Quality Research* **2012**, *12*, (3), 371-378.
- 459 27. Marple, V. A.; Liu, B. Y. H., Characteristics of laminar jet impactors. *Environ.*
460 *Sci. Technol.* **1974**, *8*, (7), 648-654.
- 461 28. Gussman, R. A., On the Aerosol Particle Slip Correction Factor. *J. Appl. Meteorol.*
462 **1969**, *8*, (6), 999-1001.
- 463 29. Zhang, Y. L.; Huang, R. J.; El Haddad, I.; Ho, K. F.; Cao, J. J.; Han, Y.; Zotter, P.;
464 Bozzetti, C.; Daellenbach, K. R.; Canonaco, F.; Slowik, J. G.; Salazar, G.; Schwikowski,
465 M.; Schnelle-Kreis, J.; Abbaszade, G.; Zimmermann, R.; Baltensperger, U.; Prévôt, A. S.
466 H.; Szidat, S., Fossil vs. non-fossil sources of fine carbonaceous aerosols in four Chinese
467 cities during the extreme winter haze episode in 2013. *Atmos. Chem. Phys. Discuss.* **2014**,
468 *14*, (19), 26257-26296.
- 469 30. Zhang, Y. L.; Zotter, P.; Perron, N.; Prévôt, A. S. H.; Wacker, L.; Szidat, S.,
470 Fossil and non-fossil sources of different carbonaceous fractions in fine and coarse
471 particles by radiocarbon measurement. *Radiocarbon* **2013**, *55*, (2-3), 1510-1520.
- 472 31. Zhang, H.; Wang, S.; Hao, J.; Wan, L.; Jiang, J.; Zhang, M.; Mestl, H. E. S.;
473 Alnes, L. W. H.; Aunan, K.; Mellouki, A. W., Chemical and size characterization of
474 particles emitted from the burning of coal and wood in rural households in Guizhou,
475 China. *Atmos. Environ.* **2012**, *51*, (0), 94-99.
- 476 32. Huang, X. F.; Yu, J. Z.; He, L. Y.; Hu, M., Size distribution characteristics of
477 elemental carbon emitted from Chinese vehicles: results of a tunnel study and
478 atmospheric implications. *Environ. Sci. Technol.* **2006**, *40*, (17), 5355-60.
- 479 33. Huang, X. F.; Yu, J. Z., Size distributions of elemental carbon in the atmosphere
480 of a coastal urban area in South China: characteristics, evolution processes, and
481 implications for the mixing state. *Atmos. Chem. Phys.* **2008**, *8*, (19), 5843-5853.

- 482 34. Cavalli, F.; Viana, M.; Yttri, K. E.; Genberg, J.; Putaud, J. P., Toward a
483 standardised thermal-optical protocol for measuring atmospheric organic and elemental
484 carbon: The EUSAAR protocol. *Atmos. Meas. Tech.* **2010**, *3*, (1), 79-89.
- 485 35. Schmid, H.; Laskus, L.; Abraham, H. J.; Baltensperger, U.; Lavanchy, V.; Bizjak,
486 M.; Burba, P.; Cachier, H.; Crow, D.; Chow, J.; Gnauk, T.; Even, A.; ten Brink, H. M.;
487 Giesen, K.-P.; Hittenberger, R.; Hueglin, C.; Maenhaut, W.; Pio, C.; Carvalho, A.;
488 Putaud, J.-P.; Toom-Sauntry, D.; Puxbaum, H., Results of the "carbon conference"
489 international aerosol carbon round robin test stage I. *Atmos. Environ.* **2001**, *35*, (12),
490 2111-2121.
- 491 36. Piazzalunga, A.; Bernardoni, V.; Fermo, P.; Valli, G.; Vecchi, R., Technical Note:
492 On the effect of water-soluble compounds removal on EC quantification by TOT analysis
493 in urban aerosol samples. *Atmos. Chem. Phys.* **2011**, *11*, (19), 10193-10203.
- 494 37. Synal, H. A.; Stocker, M.; Suter, M., MICADAS: A new compact radiocarbon
495 AMS system. *Nucl. Instr. Methods Phys. Res., Sec. B* **2007**, *259*, (1), 7-13.
- 496 38. Wacker, L.; Fahrni, S. M.; Hajdas, I.; Molnar, M.; Synal, H. A.; Szidat, S.; Zhang,
497 Y. L., A versatile gas interface for routine radiocarbon analysis with a gas ion source.
498 *Nucl. Instrum. Meth. B* **2013**, *294*, 315-319.
- 499 39. Stuiver, M.; Polach, H. A., Reporting of C-14 data - discussion. *Radiocarbon*
500 **1977**, *19*, (3), 355-363.
- 501 40. Wacker, L.; Christl, M.; Synal, H. A., Bats: A new tool for AMS data reduction.
502 *Nucl. Instr. Methods Phys. Res., Sec. B* **2010**, *268*, (7-8), 976-979.
- 503 41. Orasche, J.; Schnelle-Kreis, J.; Abbaszade, G.; Zimmermann, R., Technical Note:
504 In-situ derivatization thermal desorption GC-TOFMS for direct analysis of particle-
505 bound non-polar and polar organic species. *Atmos. Chem. Phys.* **2011**, *11*, (17), 8977-
506 8993.
- 507 42. Wang, Q.; Shao, M.; Zhang, Y.; Wei, Y.; Hu, M.; Guo, S., Source apportionment
508 of fine organic aerosols in Beijing. *Atmos. Chem. Phys.* **2009**, *9*, (21), 8573-8585.
- 509 43. Yang, F.; Huang, L.; Duan, F.; Zhang, W.; He, K.; Ma, Y.; Brook, J. R.; Tan, J.;
510 Zhao, Q.; Cheng, Y., Carbonaceous species in PM_{2.5} at a pair of rural/urban sites in
511 Beijing, 2005-2008. *Atmos. Chem. Phys.* **2011**, *11*, (15), 7893-7903.

- 512 44. Minguillón, M. C.; Perron, N.; Querol, X.; Szidat, S.; Fahrni, S. M.; Alastuey, A.;
513 Jimenez, J. L.; Mohr, C.; Ortega, A. M.; Day, D. A.; Lanz, V. A.; Wacker, L.; Reche, C.;
514 Cusack, M.; Amato, F.; Kiss, G.; Hoffer, A.; Decesari, S.; Moretti, F.; Hillamo, R.;
515 Teinila, K.; Seco, R.; Penuelas, J.; Metzger, A.; Schallhart, S.; Muller, M.; Hansel, A.;
516 Burkhart, J. F.; Baltensperger, U.; Prevot, A. S. H., Fossil versus contemporary sources
517 of fine elemental and organic carbonaceous particulate matter during the DAURE
518 campaign in Northeast Spain. *Atmos. Chem. Phys.* **2011**, *11*, (23), 12067-12084.
- 519 45. Bressi, M.; Sciare, J.; Ghersi, V.; Bonnaire, N.; Nicolas, J. B.; Petit, J. E.;
520 Moukhtar, S.; Rosso, A.; Mihalopoulos, N.; Feron, A., A one-year comprehensive
521 chemical characterisation of fine aerosol (PM_{2.5}) at urban, suburban and rural
522 background sites in the region of Paris (France). *Atmos. Chem. Phys.* **2013**, *13*, (15),
523 7825-7844.
- 524 46. Polidori, A.; Turpin, B. J.; Lim, H. J.; Cabada, J. C.; Subramanian, R.; Pandis, S.
525 N.; Robinson, A. L., Local and regional secondary organic aerosol: Insights from a year
526 of semi-continuous carbon measurements at Pittsburgh. *Aerosol Sci. Technol.* **2006**, *40*,
527 (10), 861-872.
- 528 47. Zhang, Y.-L.; Li, J.; Zhang, G.; Zotter, P.; Huang, R.-J.; Tang, J.-H.; Wacker, L.;
529 Prévôt, A. S. H.; Szidat, S., Radiocarbon-based source apportionment of carbonaceous
530 aerosols at a regional background site on hainan Island, South China. *Environ. Sci.*
531 *Technol.* **2014**, *48*, (5), 2651-2659.
- 532 48. Chen, B.; Andersson, A.; Lee, M.; Kirillova, E. N.; Xiao, Q.; Krusa, M.; Shi, M.;
533 Hu, K.; Lu, Z.; Streets, D. G.; Du, K.; Gustafsson, O., Source forensics of black carbon
534 aerosols from China. *Environ. Sci. Technol.* **2013**, *47*, (16), 9102-8.
- 535 49. Liu, J. W.; Li, J.; Zhang, Y. L.; Liu, D.; Ding, P.; Shen, C. D.; Shen, K. J.; He, Q.
536 F.; Ding, X.; Wang, X. M.; Chen, D. H.; Szidat, S.; Zhang, G., Source Apportionment
537 Using Radiocarbon and Organic Tracers for PM_{2.5} Carbonaceous Aerosols in
538 Guangzhou, South China: Contrasting Local- and Regional-Scale Haze Events. *Environ.*
539 *Sci. Technol.* **2014**, *48*, (20), 12002-12011.
- 540 50. Watson, J. G.; Chow, J. C., Source characterization of major emission sources in
541 the Imperial and Mexicali Valleys along the US/Mexico border. *Sci. Tot. Environ.* **2001**,
542 *276*, (1-3), 33-47.

- 543 51. Kaplan, I. R.; Lu, S. T.; Alimi, H. M.; MacMurphey, J., Fingerprinting of high
544 boiling hydrocarbon fuels, asphalts and lubricants. *Environmental Forensics* **2001**, *2*, (3),
545 231-248.
- 546 52. Rogge, W. F.; Hildemann, L. M.; Mazurek, M. A.; Cass, G. R.; Simoneit, B. R. T.,
547 Sources of fine organic aerosol .8. Boilers burning No. 2 distillate fuel oil. *Environ. Sci.*
548 *Technol.* **1997**, *31*, (10), 2731-2737.
- 549 53. Oros, D. R.; Simoneit, B. R. T., Identification and emission rates of molecular
550 tracers in coal smoke particulate matter. *Fuel* **2000**, *79*, (5), 515-536.
- 551 54. Rogge, W. F.; Hildemann, L. M.; Mazurek, M. A.; Cass, G. R.; Simoneit, B. R. T.,
552 Sources of Fine Organic Aerosol .2. Noncatalyst and Catalyst-Equipped Automobiles and
553 Heavy-Duty Diesel Trucks. *Environ. Sci. Technol.* **1993**, *27*, (4), 636-651.
- 554 55. Schnelle-Kreis, J.; Sklorz, M.; Peters, A.; Cyrus, J.; Zimmermann, R., Analysis of
555 particle-associated semi-volatile aromatic and aliphatic hydrocarbons in urban particulate
556 matter on a daily basis. *Atmos. Environ.* **2005**, *39*, (40), 7702-7714.
- 557 56. Schnelle-Kreis, J.; Sklorz, M.; Orasche, J.; Stolzel, M.; Peters, A.; Zimmermann,
558 R., Semi volatile organic compounds in ambient PM_{2.5}- Seasonal trends and daily
559 resolved source contributions. *Environ. Sci. Technol.* **2007**, *41*, (11), 3821-3828.
- 560 57. El-Gayar, M. S.; Abdelfattah, A. E.; Barakat, A. O., Maturity-dependent
561 geochemical markers of crude petroleums from Egypt. *Pet. Sci. Technol.* **2002**, *20*, (9-10),
562 1057-1070.
- 563 58. Czechowski, F.; Stolarski, M.; Simoneit, B. R. T., Supercritical fluid extracts
564 from brown coal lithotypes and their group components - molecular composition of non-
565 polar compounds. *Fuel* **2002**, *81*, (15), 1933-1944.
- 566 59. Fraser, M. P.; Cass, G. R.; Simoneit, B. R. T., Gas-phase and particle-phase
567 organic compounds emitted from motor vehicle traffic in a Los Angeles roadway tunnel.
568 *Environ. Sci. Technol.* **1998**, *32*, (14), 2051-2060.
- 569 60. Robinson, A. L.; Subramanian, R.; Donahue, N. M.; Bernardo-Bricker, A.; Rogge,
570 W. F., Source apportionment of molecular markers and organic aerosols-1. Polycyclic
571 aromatic hydrocarbons and methodology for data visualization. *Environ. Sci. Technol.*
572 **2006**, *40*, (24), 7803-7810.

- 573 61. Zhang, Y. X.; Schauer, J. J.; Zhang, Y. H.; Zeng, L. M.; Wei, Y. J.; Liu, Y.; Shao,
574 M., Characteristics of particulate carbon emissions from real-world Chinese coal
575 combustion. *Environ. Sci. Technol.* **2008**, *42*, (14), 5068-5073.
- 576 62. Chen, Y. J.; Sheng, G. Y.; Bi, X. H.; Feng, Y. L.; Mai, B. X.; Fu, J. M., Emission
577 factors for carbonaceous particles and polycyclic aromatic hydrocarbons from residential
578 coal combustion in China. *Environ. Sci. Technol.* **2005**, *39*, (6), 1861-1867.
- 579 63. Gelencsér, A.; May, B.; Simpson, D.; Sánchez-Ochoa, A.; Kasper-Giebl, A.;
580 Puxbaum, H.; Caseiro, A.; Pio, C.; Legrand, M., Source apportionment of PM_{2.5} organic
581 aerosol over Europe: Primary/secondary, natural/anthropogenic, and fossil/biogenic
582 origin. *J. Geophys. Res.* **2007**, *112*, (D23), D23S04.
- 583 64. Szidat, S.; Ruff, M.; Perron, N.; Wacker, L.; Synal, H.-A.; Hallquist, M.;
584 Shannigrahi, A. S.; Yttri, K. E.; Dye, C.; Simpson, D., Fossil and non-fossil sources of
585 organic carbon (OC) and elemental carbon (EC) in Goeteborg, Sweden. *Atmos. Chem.*
586 *Phys.* **2009**, *9*, 1521-1535.
- 587 65. Yttri, K. E.; Simpson, D.; Stenström, K.; Puxbaum, H.; Svendby, T., Source
588 apportionment of the carbonaceous aerosol in Norway-quantitative estimates based on
589 ¹⁴C, thermal-optical and organic tracer analysis. *Atmos. Chem. Phys.* **2011**, *11*, (17),
590 9375-9394.
- 591 66. Genberg, J.; Hyder, M.; Stenström, K.; Bergström, R.; Simpson, D.; Fors, E.;
592 Jönsson, J. Å.; Swietlicki, E., Source apportionment of carbonaceous aerosol in southern
593 Sweden. *Atmos. Chem. Phys.* **2011**, *11*, (22), 11387-11400.
- 594 67. Lu, Z.; Zhang, Q.; Streets, D. G., Sulfur dioxide and primary carbonaceous
595 aerosol emissions in China and India, 1996-2010. *Atmos. Chem. Phys.* **2011**, *11*, (18),
596 9839-9864.

597

598

599

600 **Table 1.** Sampling dates and temperature (T) of the selected aerosol samples for ^{14}C
 601 measurements and their corresponding EC concentration, fraction of modern (f_M), fraction
 602 of biomass burning (f_{BB}), fraction of fossil-fuel (f_{FF}), biomass-burning EC (EC_{BB}) and
 603 fossil-fuel EC concentrations (EC_{FF}).

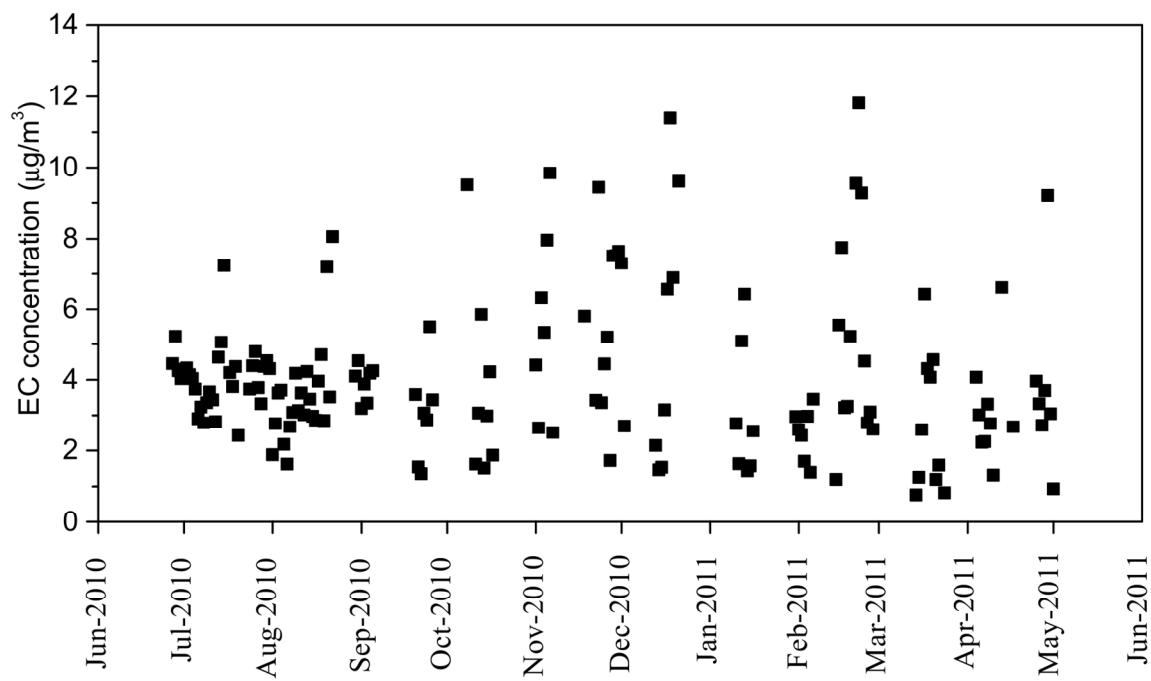
Date	T °C	EC ($\mu\text{g}/\text{m}^3$)	f_M	f_{BB}	f_{FF}	EC_{BB} ($\mu\text{g}/\text{m}^3$)	EC_{FF} ($\mu\text{g}/\text{m}^3$)
7/3/2010	30	4.30	0.15±0.02	0.14±0.02	0.86±0.02	0.59±0.07	3.7±0.46
7/5/2010	32	3.88	0.10±0.01	0.09±0.01	0.91±0.01	0.35±0.05	3.53±0.55
7/25/2010	30	4.38	0.18±0.01	0.17±0.01	0.83±0.01	0.73±0.06	3.65±0.29
7/27/2010	31	3.90	0.19±0.01	0.18±0.01	0.82±0.01	0.69±0.05	3.21±0.25
10/8/2010	17	9.50	0.25±0.02	0.23±0.02	0.77±0.02	2.19±0.21	7.31±0.7
11/28/2010	-1	7.30	0.34±0.02	0.31±0.02	0.69±0.02	2.26±0.15	5.04±0.33
11/30/2010	-1	7.64	0.28±0.02	0.25±0.02	0.75±0.02	1.95±0.13	5.7±0.39
2/15/2011	-6	5.55	0.25±0.02	0.23±0.02	0.77±0.02	1.27±0.09	4.28±0.31
2/16/2011	-3	7.75	0.25±0.02	0.23±0.02	0.77±0.02	1.77±0.13	5.98±0.45
2/21/2011	1	9.34	0.21±0.01	0.19±0.01	0.81±0.01	1.82±0.14	7.52±0.57
3/18/2011	8	4.27	0.23±0.02	0.21±0.02	0.79±0.02	0.91±0.08	3.36±0.29
3/20/2011	7	4.50	0.30±0.02	0.27±0.02	0.73±0.02	1.23±0.09	3.27±0.23
4/13/2011	17	6.61	0.26±0.02	0.24±0.02	0.76±0.02	1.59±0.13	5.02±0.4
4/30/2011	16	3.06	0.21±0.02	0.19±0.02	0.81±0.02	0.58±0.06	2.48±0.27

604 **Table 2.** Range and mean (\pm standard deviation) concentrations of hopanes (ng/m^3), picene (ng/m^3), total EC ($\mu\text{g}/\text{m}^3$), fossil-fuel EC
 605 (EC_{FF}) ($\mu\text{g}/\text{m}^3$) and picene-to- EC_{FF} emission ratio ($\text{ng}/\mu\text{g}$) in the warm and cold periods and the excess in the cold period.

Substance	Abbreviation	Warm period (n=22)		Cold period (n=15)		Excess	
		Range	Mean	Range	Mean	Mass	%
18 α (H)-22,29,30-trisnorhopane	Ts	0.39-3.80	1.52 \pm 1.18	0.93-3.69	2.21 \pm 0.85	0.69	46
17 α (H)-22,29,30-trisnorhopane	Tm	0.58-2.68	1.12 \pm 0.49	2.13-13.14	7.58 \pm 3.38	6.46	577
17 α (H),21 β (H)-30-norhopane	29ab	0.87-6.01	3.68 \pm 1.45	4.92-33.66	16.13 \pm 7.61	12.45	339
17 β (H),21 α (H)-30-norhopane+17 α (H),21 α (H)-30-norhopane	29ba	0.33-2.84	1.27 \pm 0.77	1.68-16.31	10.41 \pm 4.75	9.13	718
17 α (H),21 β (H)-30-hopane	30ab	1.33-6.68	4.14 \pm 1.53	3.03-20.64	12.60 \pm 5.61	8.45	204
17 β (H),21 α (H)-30-hopane	30ba	0.49-2.21	1.02 \pm 0.51	1.7-16.43	9.67 \pm 4.54	8.65	847
17 α (H),21 β (H)-22S-homohopane	31abS	0.69-3.35	1.98 \pm 0.78	1.62-5.14	3.31 \pm 1.16	1.33	67
17 α (H),21 β (H)-22R-homohopane	31abR	0.5-2.28	1.54 \pm 0.50	0.95-7.49	3.99 \pm 1.63	2.45	159
17 α (H),21 β (H)-22S-bishomohopane	32abS	0.63-2.45	1.52 \pm 0.48	0.94-4.43	2.89 \pm 1.02	1.37	90
17 α (H),21 β (H)-22R-bishomohopane	32abR	0.35-4.30	1.46 \pm 0.92	0.83-3.81	2.48 \pm 0.91	1.03	70
Subtotal		2.49-24.36	17.88 \pm 6.45	17.79-120.98	68.63 \pm 28.7	50.75	284
hopane index: 30ab/(30ab+30ba)		0.61-1	0.84 \pm 0.11	0.49-0.66	0.57 \pm 0.06	0.49*	
homo-hopane index: 31abS/(31abS+31abR)		0.46-0.63	0.56 \pm 0.04	0.38-0.63	0.46 \pm 0.07	0.35*	
picene		0-0.17	0.02 \pm 0.05	0.34-4.48	1.82 \pm 0.99	1.79	7576
EC [#]		3.1-9.5	4.9 \pm 2.0	5.6-9.3	7.5 \pm 1.4	2.6	52
EC _{FF} [#]		2.5-7.3	3.9 \pm 1.4	4.3-7.5	5.7 \pm 1.2	1.8	43
(picene/EC _{FF}) [#]		0-0.09	0.02 \pm 0.03	0.24-0.41	0.34 \pm 0.07	1.0*	

606 * These ratios are determined from the masses of the individual components for the excess in the cold period.

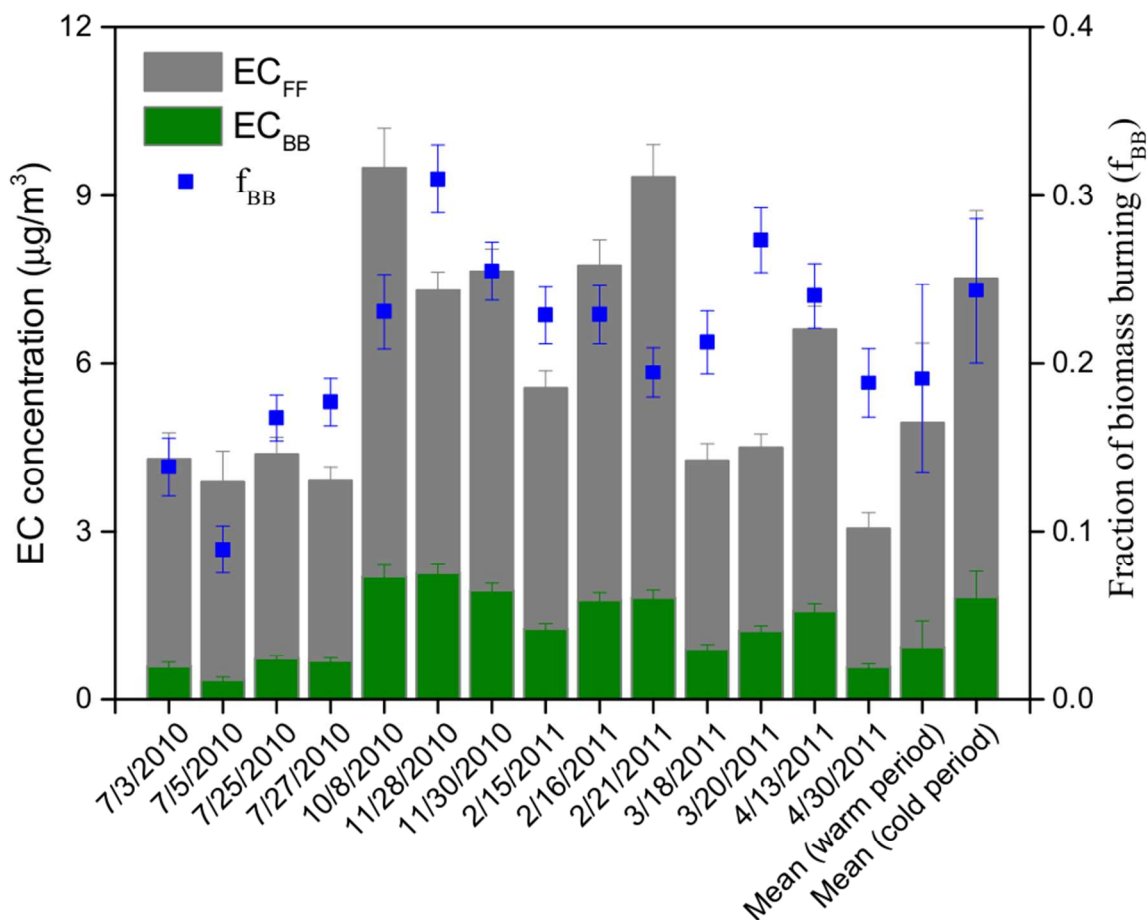
607 # The values are obtained from a subset of samples, which are measured for radiocarbon (n=9 and 5 for the warm and cold periods, respectively).



608

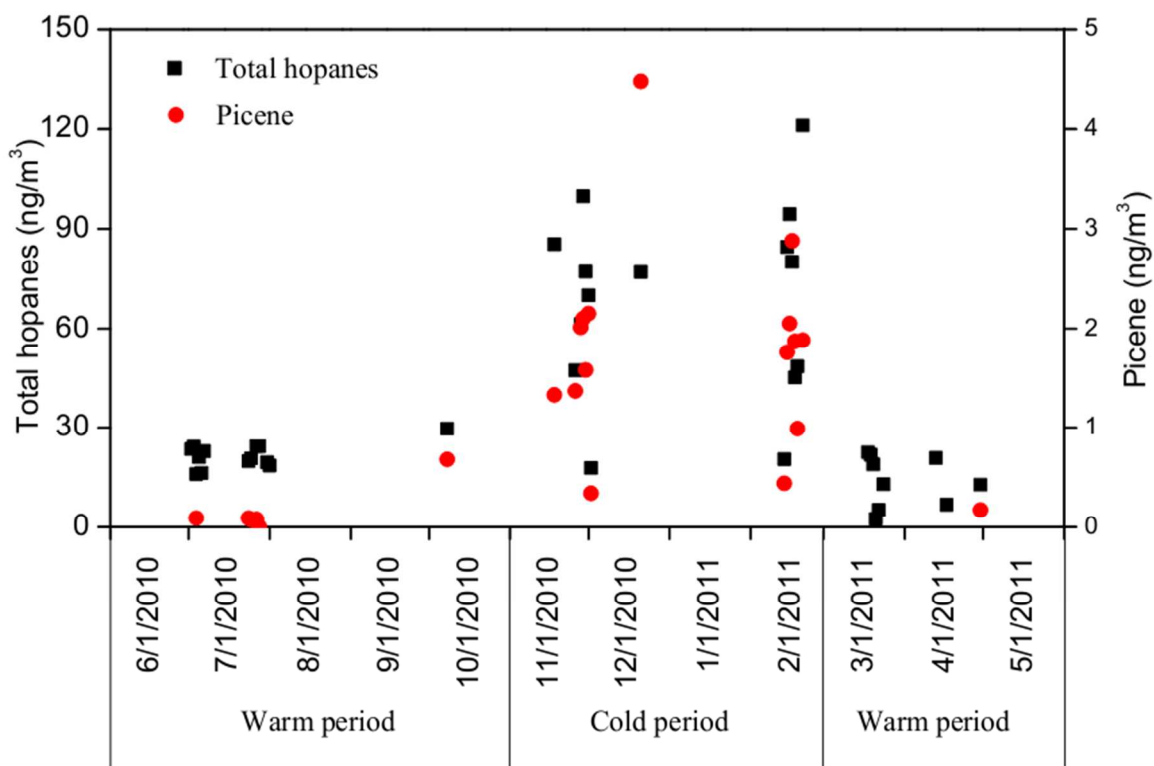
609 **Figure 1.** Temporal variation of EC concentrations ($\mu\text{g}/\text{m}^3$, $n=155$) in Beijing, China.

610



611

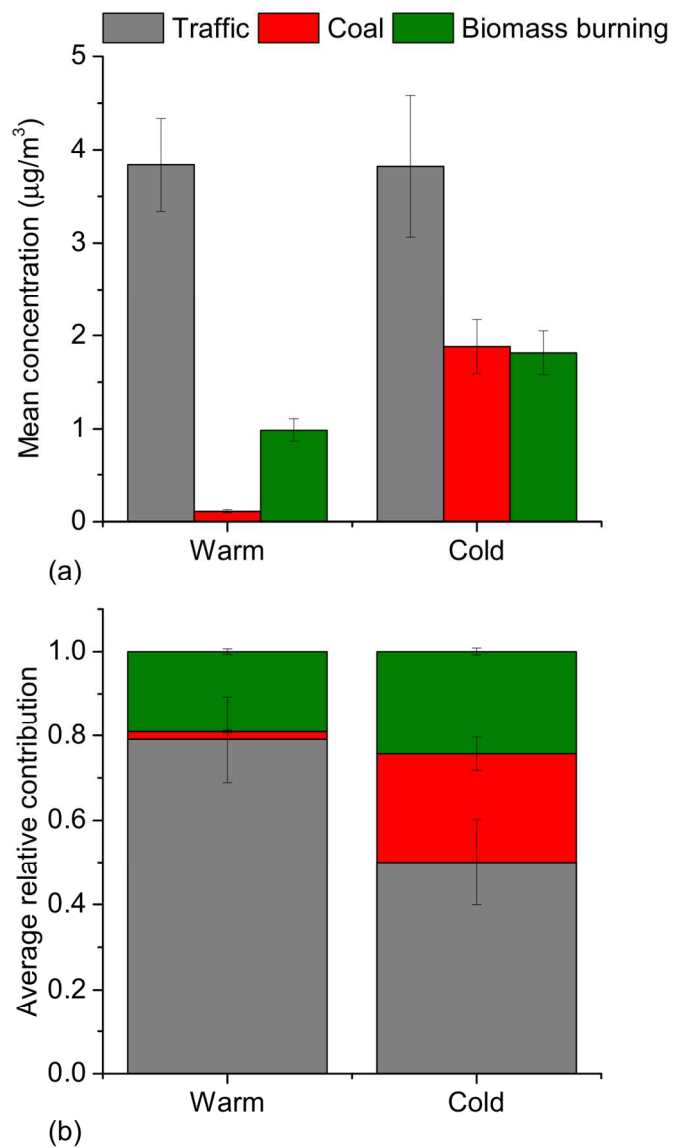
612 **Figure 2.** Mass concentrations ($\mu\text{g}/\text{m}^3$) of EC from biomass burning and fossil-fuel
 613 combustion (EC_{BB} and EC_{FF}, respectively) as well as fractions of biomass-burning EC to
 614 total EC (f_{BB}) in Beijing with 1 σ uncertainties.



615

616 **Figure 3.** Temporal variation (n=35) of total identified hopanes (see in Table 2) and
617 picene concentrations (ng/m³) in Beijing, China. The interval of x-axis is 30 days.

618



619

620 **Figure 4.** Average EC concentrations (a) and relative contributions (b) from traffic-
 621 related, coal and biomass-burning emissions in the warm (March to October) and cold
 622 (November to February) periods. Uncertainty bars represent 10th and 90th percentiles
 623 from LHS calculations. The integrated probability distribution and sensitivity test (with a
 624 variation of $((\text{picene}/\text{EC})_{\text{coal}})$ from the LHS simulation is shown in the Figure S3 and S4
 625 (see Supporting Information).

626